Macromolecular Materials and Engineering

Macromolecular Materials and Engineering Open Access

www.mame-journal.de

RESEARCH ARTICLE OPEN ACCESS

Influence of Viscosity Ratio on the Mechanical, Morphological, and Rheological Properties of Thermoplastic Dynamic Vulcanizates from Devulcanized Tire Rubber and Polypropylene

Ákos Görbe[1,2] | Gergő Zsolt Marton[1,3] | Tamás Bárány[1,2,4]

[1]Department of Polymer Engineering, Faculty of Mechanical Engineering, Budapest University of Technology and Economics, Műegyetem rkp. 3., Budapest, Hungary | [2]PolymerOn Ltd., Háros u. 7., Budapest, Hungary | [3]MTA-BME Lendület Sustainable Polymers Research Group, Műegyetem rkp. 3., Budapest, Hungary | [4]MTA-BME Lendület Lightweight Polymer Composites Research Group, Műegyetem rkp. 3., Budapest, Hungary

Correspondence: Tamás Bárány (barany.tamas@gpk.bme.hu)

Received: 28 May 2025 | **Revised:** 5 August 2025 | **Accepted:** 5 August 2025

Funding: Project no. KDP-IKT-2023-900-I1-00000957/0000003 has been implemented with the support provided by the Ministry of Culture and Innovation of Hungary from the National Research, Development and Innovation Fund, financed under the KDP-2023 funding scheme. This research was funded by the National Research, Development and Innovation Office, Hungary (2021-1.1.4-GYORSÍTÓSÁV-2022-00030). Project no. TKP-6-6/PALY-2021 has been implemented with the support provided by the Ministry of Culture and Innovation of Hungary from the National Research, Development and Innovation Fund, financed under the TKP2021-NVA funding scheme.

Keywords: damage behavior | devulcanization | polypropylene | rheology | thermoplastic dynamic vulcanizates

ABSTRACT

In this study, we examined the effect of matrix viscosity on the properties of thermoplastic dynamic vulcanizates (TDV) produced using devulcanized ground tire rubber (dGTR) and polypropylene (PP). Polypropylenes with substantially different MFI were used to demonstrate the effect of viscosity on the properties of the resulting TDV. We examined the temperature dependence of the viscosity ratio of the components during dynamic vulcanization and found that if the viscosity of PP is closer to that of the dGTR blend, more time is allowed for the crosslinked rubber particles to disperse. We examined the TDVs thoroughly, performing tensile, acoustic emission, falling weight tests, morphological, and rheological analysis. We found a clear trend between scorch viscosity ratio and the main mechanical properties: all properties improved with increasing scorch viscosity ratio. We also found a significant decrease in rubber grain size distribution in connection with the increasing matrix viscosity, leading to improved toughness.

1 | Introduction

The recycling of polymeric materials imposes great challenges, and while thermoplastic materials can be recycled via remelting and reshaping [1, 2], other strategies have to be considered when dealing with elastomers, where the crosslinks block reversible melting [3–8]. Waste tires pose the most pressing issue in this field: the amount of them is estimated to be more than 1 billion tires annually [5]. Tire rubber can be shredded to produce ground tire rubber (GTR) [9]. GTR is widely utilized as a cost-effective and sustainable filler or modifier in various applications, including asphalt pavements, flooring, playground surfaces, and polymer materials. Its reuse not only mitigates landfill accumulation and conserves natural resources but also improves key material properties such as impact resistance, damping performance, and overall durability. Incorporating GTR

TABLE 1 | Materials used for curing the rubber phase of the TDV.

Material	Manufacturer	Trademark	Function
ZnO	Werco Metal (Zlatna, Romania)	—	Activator
stearic acid	Oleon (Ertvelde, Belgium)	Radiacid 0154	
CBS N-cyclohexyl-2-benzothiazolesulfenamide	Rhein Chemie (Mannheim, Germany)	Rhenogran CBS-80	Accelerator
sulfur	Ningbo Actmix Polymer (Ningbo, Zhejiang, China)	ACTMIX S-80	Curing agent

TABLE 2 | Recipe for the rubber phase.

	Amount of ingredient (phr)
dGTR	100
ZnO	5
stearic acid	2
CBS	1.5
Sulfur	1.5

TABLE 3 | Formulation of the compounds.

Compound	Components
TDV_MFI2	40 wt% PP R660 + 60 wt% dGTR mixture
TDV_MFI12	40 wt% PP R359 + 60 wt% dGTR mixture
TDV_MFI45	40 wt% PP R959 + 60 wt% dGTR mixture

TABLE 4 | Parameters for injection molding.

Temperature profile [°C]	190/190/185/180/175/45
Dosage [cm^3]	45
Residual cooling time [s]	20
Injection rate [cm^3/s]	25
Back pressure [bar]	40
Mold temperature [°C]	30

into thermoplastics or elastomers aligns with circular economy principles by extending the service life of rubber-based materials. Among the various reuse strategies, one of the most promising is the integration of GTR into new rubber products or its application as a reinforcing filler in thermoplastic matrices. This practice is well-established and primarily pursued to enhance the toughness and mechanical resilience of thermoplastic polymers [10–13]. The incompatibility between GTR and thermoplastic matrices results in a material with inferior mechanical properties: to achieve satisfactory mechanical performance, the application of compatibilization strategies is essential [14–17].

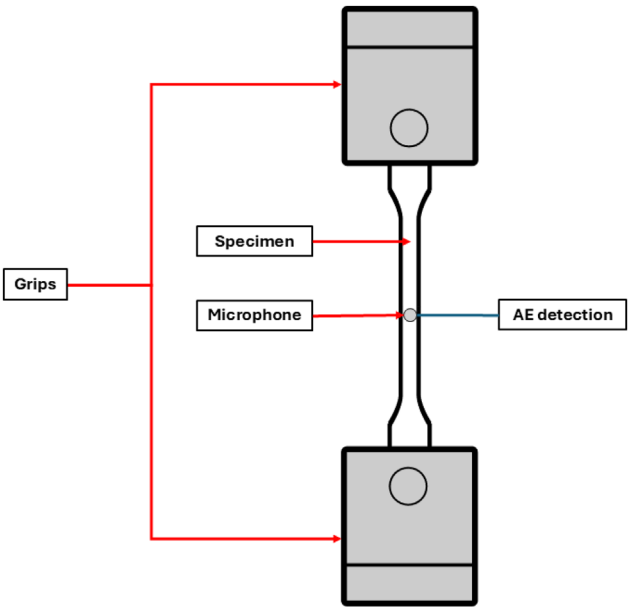

FIGURE 1 | Measurement setup for detecting acoustic emission signals [42].

The interfacial connection of GTR and the matrix can be improved with devulcanization and reclamation: a process that aims to break the crosslinks of an elastomer with directed energy and results in a reprocessable material. Various methods exist, with the most prevalent being thermomechanical [18–21], thermochemical [22], and microwave devulcanization [23, 24]. Devulcanized ground tire rubber (dGTR) and GTR can be blended with thermoplastic polymers to develop thermoplastic elastomers (TPE). TPEs exhibit rubber-like behavior due to their physical crosslinked structure while being reversibly meltable, granting recyclability [25]. One group of TPEs is polymer-elastomer blends, which gain rubbery behavior from finely dispersed rubber domains in a thermoplastic matrix [12, 26]. The particle size of the rubber phase is essential to be in the micrometer range for rubber-like behavior, which can be achieved via dynamic vulcanization [27, 28]. In this process, the unvulcanized rubber mixture is fed into the processing equipment; vulcanization occurs in situ during the compounding under intensive shearing [29, 30]. It reduces the size of the rubber domains, resulting in thermoplastic dynamic vulcanizate (TDV). The most popular and commercially

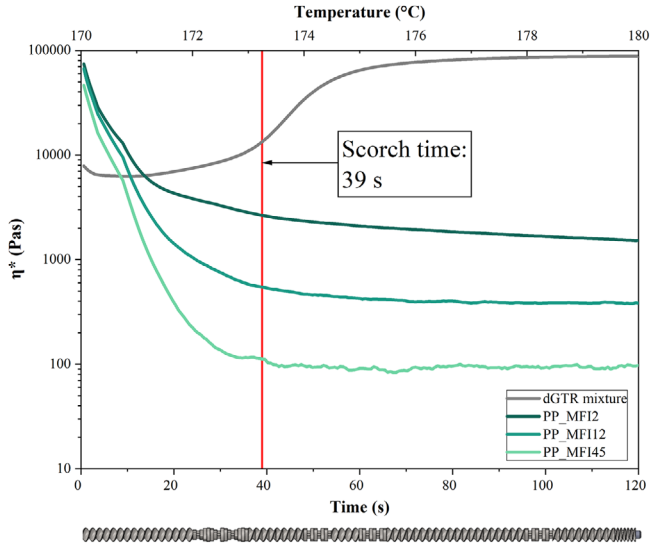

FIGURE 2 | Change of the complex viscosity of the neat PPs and the dGTR mixture as a function of temperature.

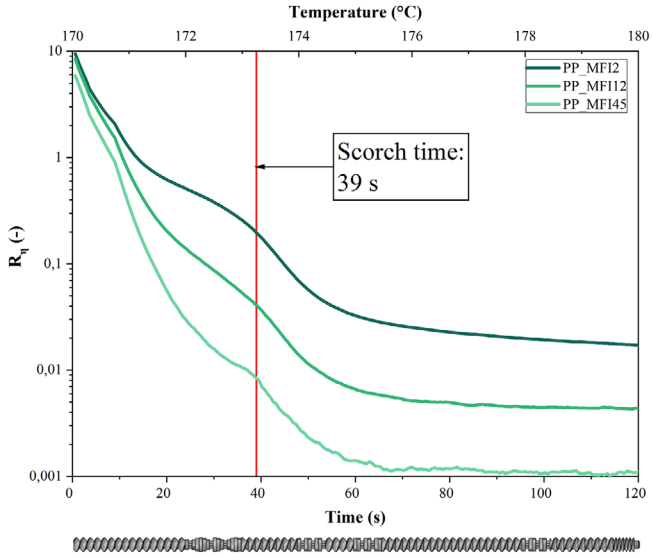

FIGURE 3 | Change of the viscosity ratio of the neat PPs and the dGTR mixture as a function of temperature.

available TDVs are composed of polypropylene (PP) and ethylene propylene diene monomer rubber (EPDM). Using dGTR as the rubber phase of TDVs creates an opportunity to upcycle waste tires as high-tech and recyclable materials that can be inserted into the circular economy [31–34].

Several studies have shown that the mechanical properties of TDVs depend on numerous factors, one of which is the properties of the thermoplastic phase. Blend ratio was inspected, and it was found that the increase in the rubber phase facilitates better elasticity [35, 36]. The molecular weight and viscosity of the thermoplastic phase also play an important role in the properties of TDVs: it was reported that an increase in viscosity results in smaller rubber domains [27, 37]. This occurs because higher viscosity enhances the transfer of shear stress from the matrix to the rubber phase, facilitating more efficient distribution of rubber domains [38]. However, high molecular weight may also result in the increase of rubber domain sizes during dynamic vulcanization: higher viscous dissipation can increase the temperature of the system and the crosslinking reaction rate as well [37]. In this work, we investigated the effect of matrix viscosity in TDVs based on PP and dGTR. While several studies have established the influence of matrix viscosity on the morphology and mechanical properties of TDVs based on virgin rubber, limited attention has been given to systems incorporating recycled rubber. Given the distinct characteristics of dGTR—such as its partially broken crosslinked structure and heterogeneous composition—it remains unclear whether the viscosity–property relationships observed in traditional TDVs hold true for these more complex, recycled systems. Our aim was to address this gap by systematically evaluating whether the established trends in literature are applicable to PP/dGTR-based TDVs.

2 | Materials and Methods

2.1 | Materials

We used several polypropylene grades with three distinct viscosities to conduct our experiments, all provided by MOL Petrochemicals Ltd. (Tiszaújváros, Hungary). We used:

- PP R660 (labeled as PP_MFI2) random PP copolymer (extrusion grade, MFI (2.16 kg, 230°C) 2 g/10 min),
- PP R359 (labeled as PP_MFI12) random PP copolymer (injection molding grade, MFI (2.16 kg, 230°C) 12 g/10 min),
- PP R959 (labeled as PP_MFI45) random PP copolymer (injection molding grade, MFI (2.16 kg, 230°C) 45 g/10 min),

Devulcanized ground tire rubber (dGTR) was provided by Tyromer Inc. (Waterloo, ON, Canada). Ground tire rubber, made from truck tires with a particle size under 1 mm, is thermomechanically devulcanized in an extruder with the help of supercritical CO_2.

The curatives and additives in the rubber phase of the TDVs are listed in Table 1.

2.2 | Preparation of TDVs

We prepared the rubber phase of the TDVs using a Brabender Lab-Station internal mixer (Brabender GmbH & Co. KG (Duisburg, Germany)) equipped with a W 350 E chamber (free volume 370 cm^3). The temperature was set to 50°C, and the batches were mixed at 40 rpm. Table 2 shows the recipe for the rubber phase.

We prepared the compounds with a Labtech Engineering LTE 26–44 co-rotating twin-screw extruder (Labtech Engineering Co., Ltd., Samutprakarn, Thailand, screw diameter: 44 mm) with a revolution speed of 120 rpm. The compositions of the compounds are listed in Table 3. We have named the TDVs according to the MFI values of the PPs.

We prepared flat and dumbbell specimens of both the TDVs and the reference PPs by injection molding using an Arburg

TABLE 5 | Key properties of the TDVs of different flow grade PPs.

	Tensile strength (MPa)	Strain at break (%)	Perforation energy (J/mm)	Scorch viscosity ratio (-)
TDV_MFI2	9.5 ± 0.5	125.1 ± 12.3	4.6 ± 1.1	0.1980
TDV_MFI12	8.5 ± 0.1	85.1 ± 5.3	3.5 ± 1.1	0.0409
TDV_MFI45	7.2 ± 0.2	36.7 ± 3.2	1.9 ± 0.1	0.0084
PP_MFI2	14.9 ± 0.3	46.6 ± 2.2	16.1 ± 0.5	—
PP_MFI12	15.4 ± 0.2	48.4 ± 4.5	15.2 ± 0.5	—
PP_MFI45	28.0 ± 1.3	9.7 ± 0.6	1.8 ± 0.8	—

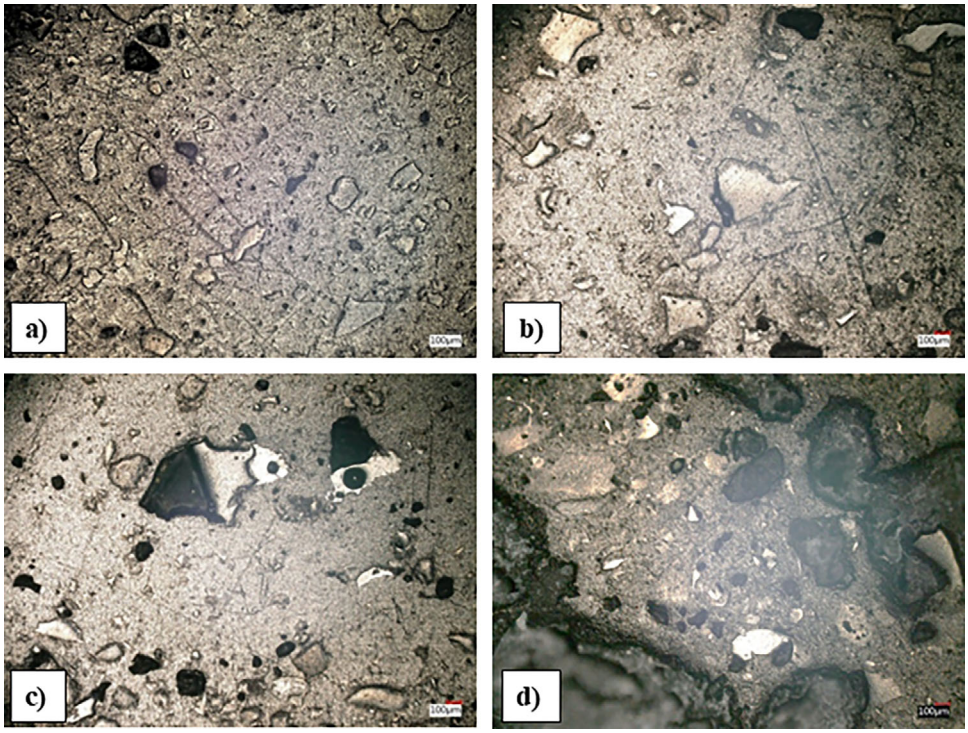

FIGURE 4 | Morphology of the TDVs of different flow grade PPs (a): TDV_MFI2, (b): TDV_MFI12, (c): TDV_MFI45, (d): neat dGTR.

Allrounder Advance 270S 400-170 type (Arburg GmbH, Lossburg, Germany) injection molding machine with a temperature profile of 190/190/185/180/175/45°C (Table 4).

2.3 | Testing Methods

We studied the dynamic vulcanization process with a MonTech D-RPA 3000 (MonTech (Buchen, Germany)) rubber process analyzer. This machine can register the change in viscosity of both phases. We characterized the specimens with an anisotherm test executed between 170 and 180°C with 10°C/min of heating speed to model the temperature profile of extrusion. We defined the temperature-dependent viscosity ratio according to Equation (1):

$$R_\eta(T) = \frac{\eta_{PP}(T)}{\eta_{mixture}(T)} \quad (1)$$

where $R_\eta(T)$ is the viscosity ratio at a given temperature (-), $\eta_{PP}(T)$ is the complex viscosity of the PP phase at a given temperature and $\eta_{mixture}(T)$ is the complex viscosity of the rubber phase at a given temperature.

We performed tensile tests (according to ISO 37, Type 2 dumbbell specimens) on standardized specimens. A Zwick Z005 (Zwick GmbH (Ulm, Germany)) universal testing machine equipped with a 5 kN load cell was used with a 100 mm/min crosshead speed.

We used the acoustic emission (AE) method to acquire the acoustic waves generated by the damage mechanisms of the material. The analysis of different AE signal properties enables the characterization of the damage and failure process [39–41]. The AE signals were recorded during tensile tests in a measurement setup shown in Figure 1. We conducted the measurements with a Mistras PCI-2 (MISTRAS Group, Princeton Junction, USA) AE system in connected with an IL40S preamplifier (Physical

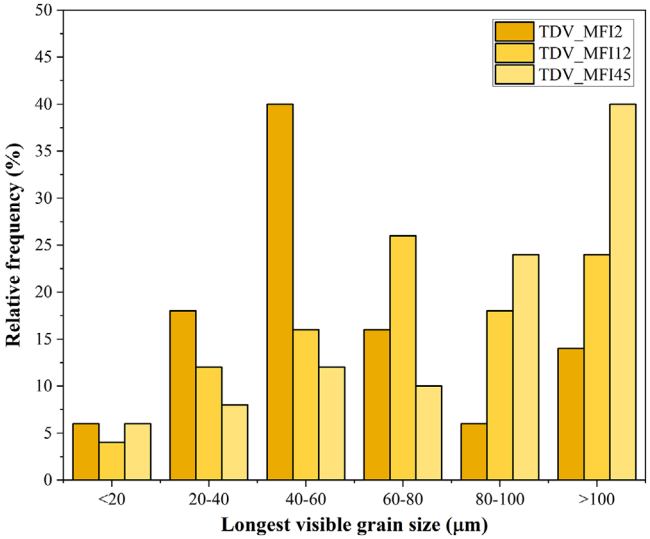

FIGURE 5 | Grain size distribution in the TDVs of different flow grade PPs.

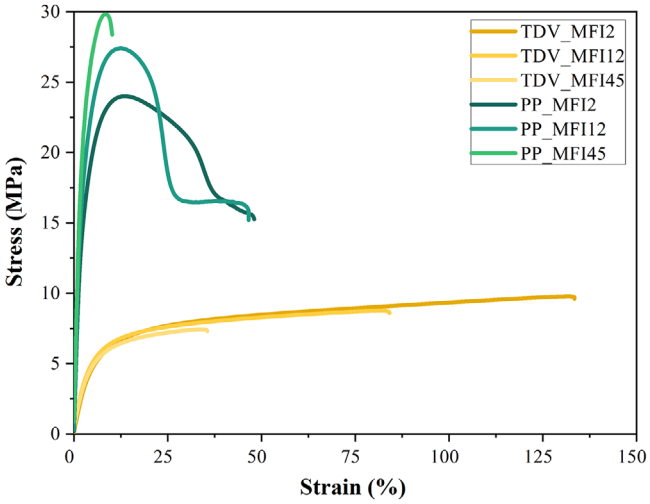

FIGURE 6 | Characteristic tensile curves of the TDVs of different flow grade PPs.

Acoustic Corporation, Princeton Junction, USA) with a gain of 40 dB and a Micros30s (Physical Acoustic Corporation, Princeton Junction, USA) microphone (operating frequency range: 150–400 kHz). To ensure proper connection between the sensor and the specimen, we used Oxett silicon grease (T-Silox Ltd., Budapest, Hungary) as a coupling agent. We set a 30 dB threshold for the measurements to filter out ambient noises according to previous experience [37, 38]. The evaluation of the acoustic emission testing results was carried out with Noesis 9.0 and MATLAB R2024b software.

We used a Keyence VHX-5000 (Keyence Corporation (Mechelen, Belgium)) light microscope for the determination of grain size distribution of the TDV samples. A distribution diagram was created based on measuring the largest visible size of 100 rubber particles using the ImageJ software.

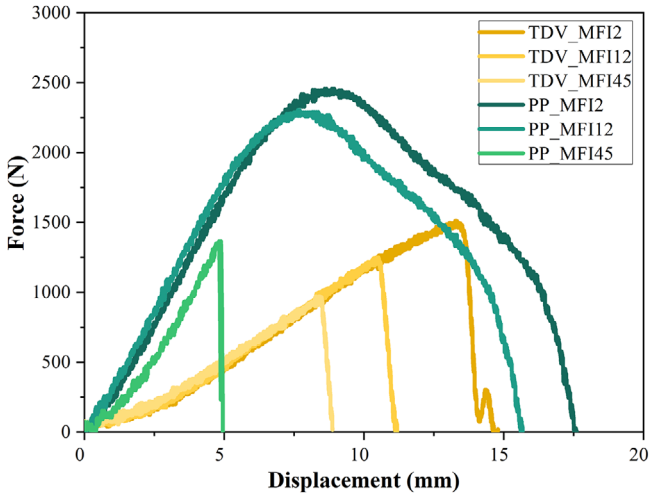

FIGURE 7 | Characteristic falling weight curves of the TDVs of different flow grade PPs.

We performed all microscopical examinations on welded specimens embedded in epoxy resin. We polished these samples using a Struers LaboPol-5 (Struers A/S, Netherlands) in 7 steps according to the manufacturer's advice.

The injection molded specimens were characterized by instrumented falling-weight impact tests performed with a Ceast Fractovis 9350 falling-weight impact testing machine (Instron, Torino, Italy) at room temperature according to ISO 6603. The total mass of the dart was 19.5 kg, the drop height was 1 m, the impact energy was 200.2 J, the diameter of the dart was 20 mm, and a 40 mm diameter supporting ring was used to clamp the 80 mm × 80 mm square specimens.

The melt rheology of the specimens was examined using a Netzsch Kinexus Prime pro+ rotational rheometer (Netzsch Group, Selb, Germany) at 190°C. We performed an amplitude sweep between 0.1 and 100% strain to determine the linear viscoelastic region. After that, we performed a frequency sweep between 0.1 and 100 Hz at 1% strain.

3 | Results and Discussion

3.1 | Viscosity Ratio and Change During Dynamic Vulcanization

The viscosity and viscosity ratio of the tested materials were measured in an oscillating rheometer. The temperature profile is identical to that used in dynamic vulcanization, so that the change in viscosity and viscosity ratio of the TDV components during dynamic vulcanization can be modelled.

Two different trends are observed when examining the temperature dependence of the viscosities (Figure 2). While the complex viscosity of the dGTR mixture increases with increasing temperature as crosslinks are formed, the viscosity of PPs decreases until a plateau is reached. The plateau viscosity of the PPs indicates the

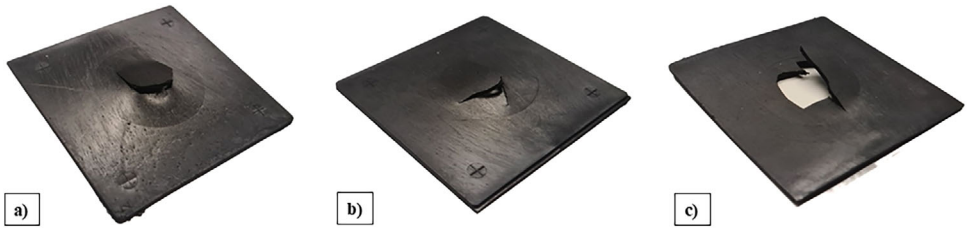

FIGURE 8 | Specimens after falling weight tests (a) TDV_MFI2, (b) TDV_MFI12, (c) TDV_MFI45.

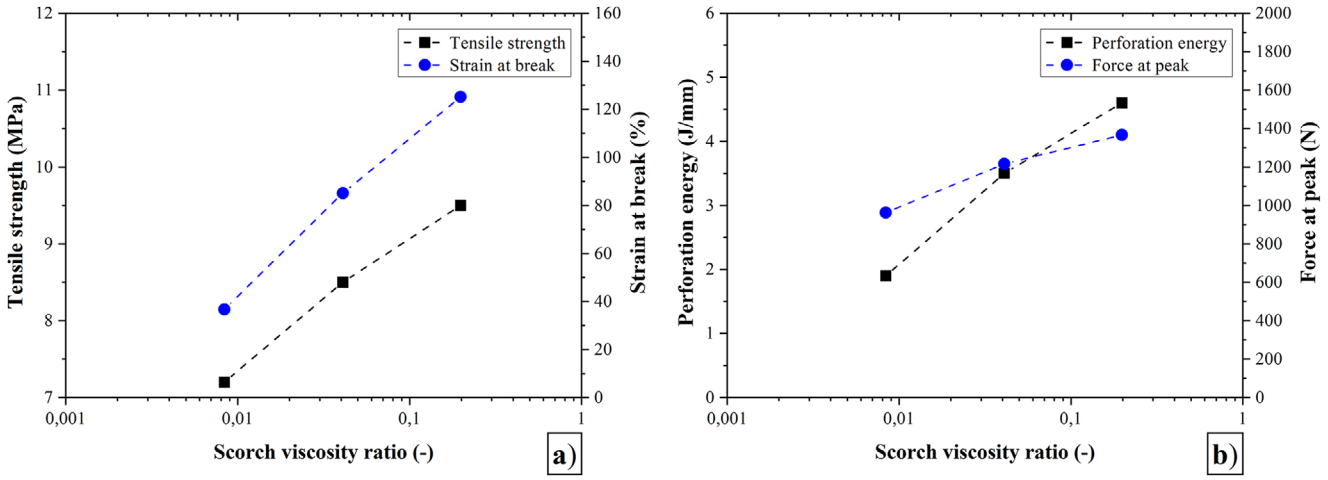

FIGURE 9 | The scorch viscosity ratio dependence of the main material properties (a) tensile properties, (b) energy absorption.

steady-state viscosity of the melt, which matches the MFI values in the datasheets: PP_MFI2 has the highest viscosity, PP_MFI12 the lowest, PP_MFI45 in between. It can also be seen that the reduction of the viscosity of PP_MFI45 is the most pronounced, while PP_MFI2 is characterized by the smallest drop. This can be in connection with the molecular mass and chain length of the polymer: higher molecular mass might provide less viscosity loss on heating [43–45]. We also experienced a kind of "noise" on the curve of PP_MFI45. This can be in connection with the instability of the polymer melt caused by the high flowability of the material.

The change of viscosity ratio during dynamic vulcanization shows a downward trend (Figure 3). This is caused by the drastic reduction of the viscosity of PP as a result of heating. A step that can be linked to the vulcanization of the rubber can be observed on all three curves. If the viscosity curve (Figure 2) of the PP is closer to that of the dGTR mixture, this step is more pronounced and can be seen over a wider range of temperatures. This wider step can provide an opportunity to increase the efficiency of dynamic vulcanization: if the rubber particles encounter a matrix of higher viscosity before their scorch time, the shear exerted by the matrix may break the particles up better. After the vulcanization is completed, a decrease can be observed since the viscosity of the rubber phase does not change. We introduced the scorch viscosity ratio measured at the scorch time of the rubber phase (scorch viscosity ratio). This parameter can quantify the effectiveness of the dynamic vulcanization, as the breakup of the rubber domains typically occurs before the scorch time. It can be seen in Table 5 that the scorch viscosity ratio follows a logarithmic decrease.

3.2 | Morphology

Light microscope pictures (Figure 4) and the grain size distribution (Figure 5) of the TDVs illustrate their morphological properties. It is clear that the decrease in viscosity results in a shift towards larger particle size ranges. This correlates well with results from the literature, many researchers have shown before that conventional TDVs with a thermoplastic phase of higher viscosity can produce a higher shear rate due to their higher melt strength. This increased shear is, in turn, capable of improving the distribution of the rubber particles.

It is important to note that the results may be distorted by the nature of neat dGTR. It can be seen in Figure 4/d that the dGTR is not homogeneously devulcanized but can be described as a devulcanizate-GTR mixture with GTR particles above 100 µm. These large particles can be observed in the TDVs as well, since they cannot be broken up effectively due to their crosslinks.

3.3 | Tensile Tests

The results of the tensile tests (Figure 6, Table 5) show a clear tendency: the tensile curves of the TDVs are extended significantly if the scorch viscosity ratio increases; a higher viscosity ratio ensures better dispersion as seen from the grain size distribution diagram (Figure 5), which results in improved elasticity with enhanced strain at break. Decreasing matrix viscosity causes worse dispersion, and large rubber particles act as a source of failure and worsen the mechanical characteristics. However, it can also be observed that none of the curves exhibit any signs

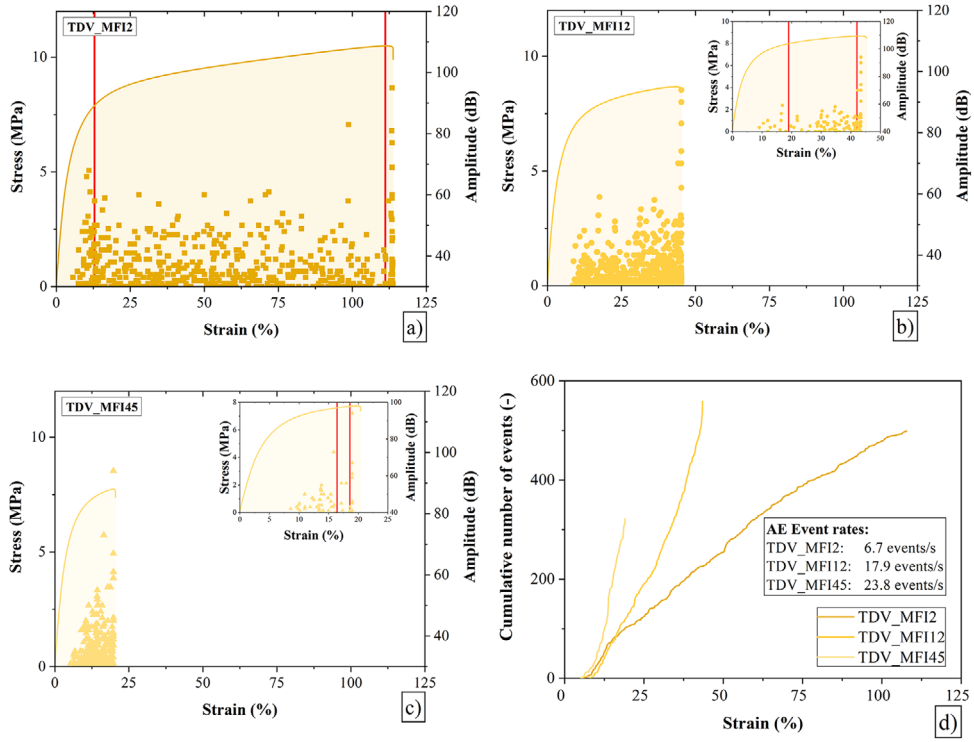

FIGURE 10 | Combined tensile-amplitude (a: TDV_MFI$_2$, b: TDV_MFI$_{12}$, c: TDV_MFI$_{45}$) and cumulative number of events curves (d) of the TDVs.

of neck formation, so that TDV-like characteristics could be achieved with all three materials. A comparison of the tensile strength curves of the three PPs shows that the strain at break of the materials themselves does not differ significantly, except for PP_MFI45. This suggests that it is indeed the change in viscosity that causes the improvement in the properties of the TDVs.

3.4 | Falling Weight Impact Tests

The results of the falling weight impact tests (Figure 7, Table 5) show that the matrix viscosity directly affects the energy absorption of the samples: increasing viscosity results in an increase of both maximum force and displacement, and the perforation energy as a consequence. This can be explained by the better dispersion provided by higher viscosity. It can be seen from test curves that the neat PPs behaved similarly under these loads, apart from PP_MFI45. This behavior also supports the idea that the improvement seen in TDV properties is due to the change in PP viscosity and the resulting morphological changes.

A change in the form of the failure can also be identified as a cause of the increasing perforation energy. In Figure 8, it can be observed that the highest viscosity and molecular weight PP was able to induce a break that resulted in a significant out-of-plane deformation. Conversely, with decreasing viscosity, the out-of-plane deformation decreases until catastrophic failure occurs (Figure 8/c).

Table 5 and Figure 9 show that there is a clear correlation between the scorch viscosity ratio and the key properties of the TDV: it can be seen that tensile strength, strain at break, and perforation energy all increase linearly with increasing viscosity ratio. This is all in connection with the improvement of the grain size distribution; numerous studies in the literature have shown the grain size dependence of these properties [46–48]. According to the generally accepted failure theory of TDVs, the damage starts at the rubber-thermoplastic interphase, and the failure occurs through localized yielding of the matrix [49]. If the grain size decreases, resulting interlaminar voids are less likely to coalesce, thus prolonging failure [27, 50]. This effect may also occur when subjected to complex, out-of-plane loads during falling weight tests.

3.5 | Acoustic Emission Analysis

In line with our previous studies [42], the behavior of the TDVs during tensile deformation can be divided into three characteristic stages based on the number and amplitude of acoustic emission signals marked by red lines in Figures 10a, b, and c. During the elastic deformation stage, only a few AE signals are detected, typically with amplitudes ranging from 30 to 60 dB. These events are likely associated with initial yielding in the matrix ligaments and localized phase separation at the weakest interfacial regions. The end of the first stage is usually marked by the appearance of the first high-amplitude signal. In the plastic deformation region, the number of signals increases markedly, while their amplitudes generally remain below 50 dB. This increase is attributed to the progressive debonding between the polypropylene and rubber phases. Consistent with our earlier findings, the low energy requirement for this separation, due to their limited compatibility, results in low-amplitude signals. Finally, the macroscopic fracture is indicated by a distinct high-amplitude signal exceeding 90 dB, accompanied by echoes.

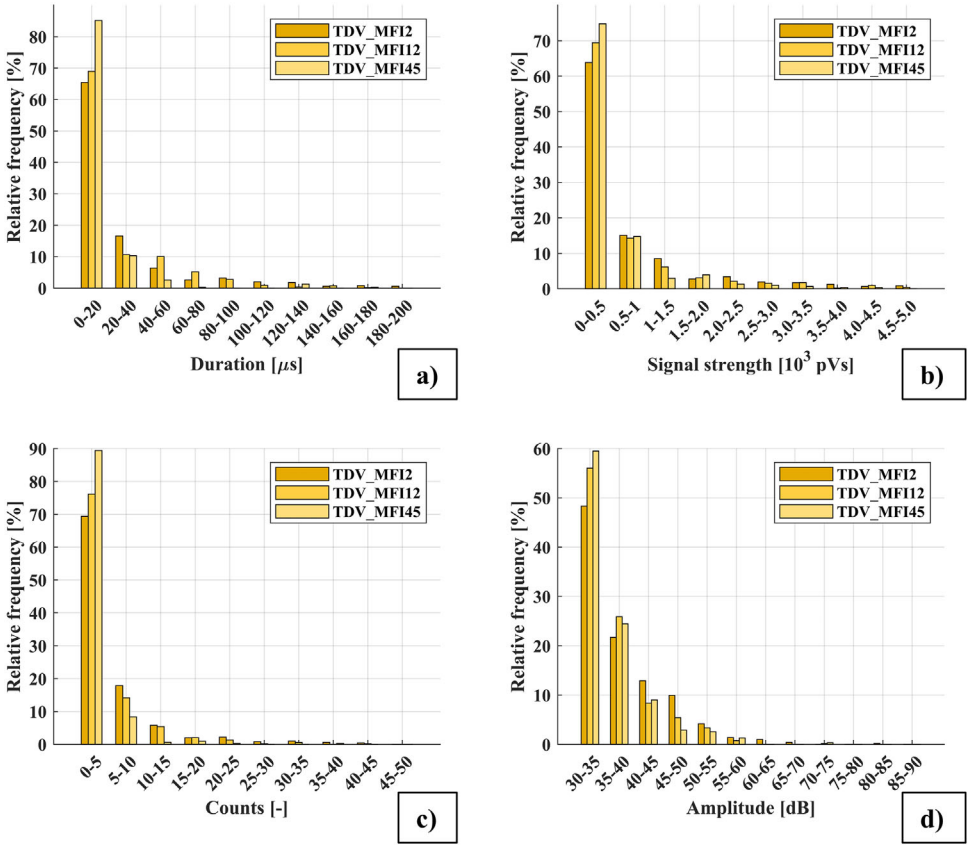

FIGURE 11 | Duration (a), signal strength (b), counts (c), and amplitude (d) distribution of the signals emitted during the tensile tests.

The AE measurements revealed that the end of the first stage of failure occurs at approximately the same strain for all three materials, as this stage is dominated by the behavior of the polypropylene phase. However, the length of the second stage correlates with the viscosity of the matrix: the particle size reduction achieved with increasing matrix viscosity leads to a prolonged second stage, which is associated with more effective toughening. The smaller particle size alters the failure mechanism, enabling higher strain at break even without compatibilization. This is also well reflected in the cumulative number of events–strain curves and the event rate values (

Figure 10/d): The TDV with the smallest particle size exhibits a much flatter curve compared to the other two materials, lacking the steep, upward inflection at the end that typically indicates abrupt failure. Instead, the curve transitions more gradually, indicating a slower and more ductile failure process.

We analyzed the properties of the acoustic signals, excluding the failure stage was as it refers to the global failure instead of the formation and propagation of damage inside the material. The enhanced toughening effect associated with smaller particle sizes is also reflected in the acoustic signal characteristics (Figure 11): with decreasing particle size, the characteristic values of all signal properties shift toward higher values. Particle size reduction increases signal duration (Figure 11/a), indicating longer events and a more gradual failure process. Additionally, the signal strength tends to increase with decreasing particle size (Figure 11/b), which may be related to the larger specific surface area: smaller rubber particles form interfaces with the matrix

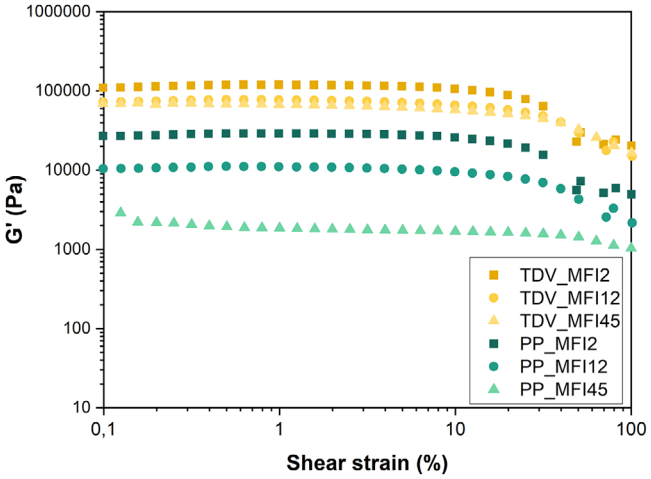

FIGURE 12 | Amplitude dependence of storage modulus.

over a greater total area. This phenomenon also results in higher signal amplitudes and counts (Figure 11/c and d), indicating higher intensity and complexity of the signals associated with the damage mechanisms of the material with enhanced toughness.

3.6 | Melt Rheology

From the results of the amplitude sweeps (Figure 12), it can be observed that the G' curve associated with TDV_MFI2 runs above the curves of the other TDVs. This indicates a higher elasticity due

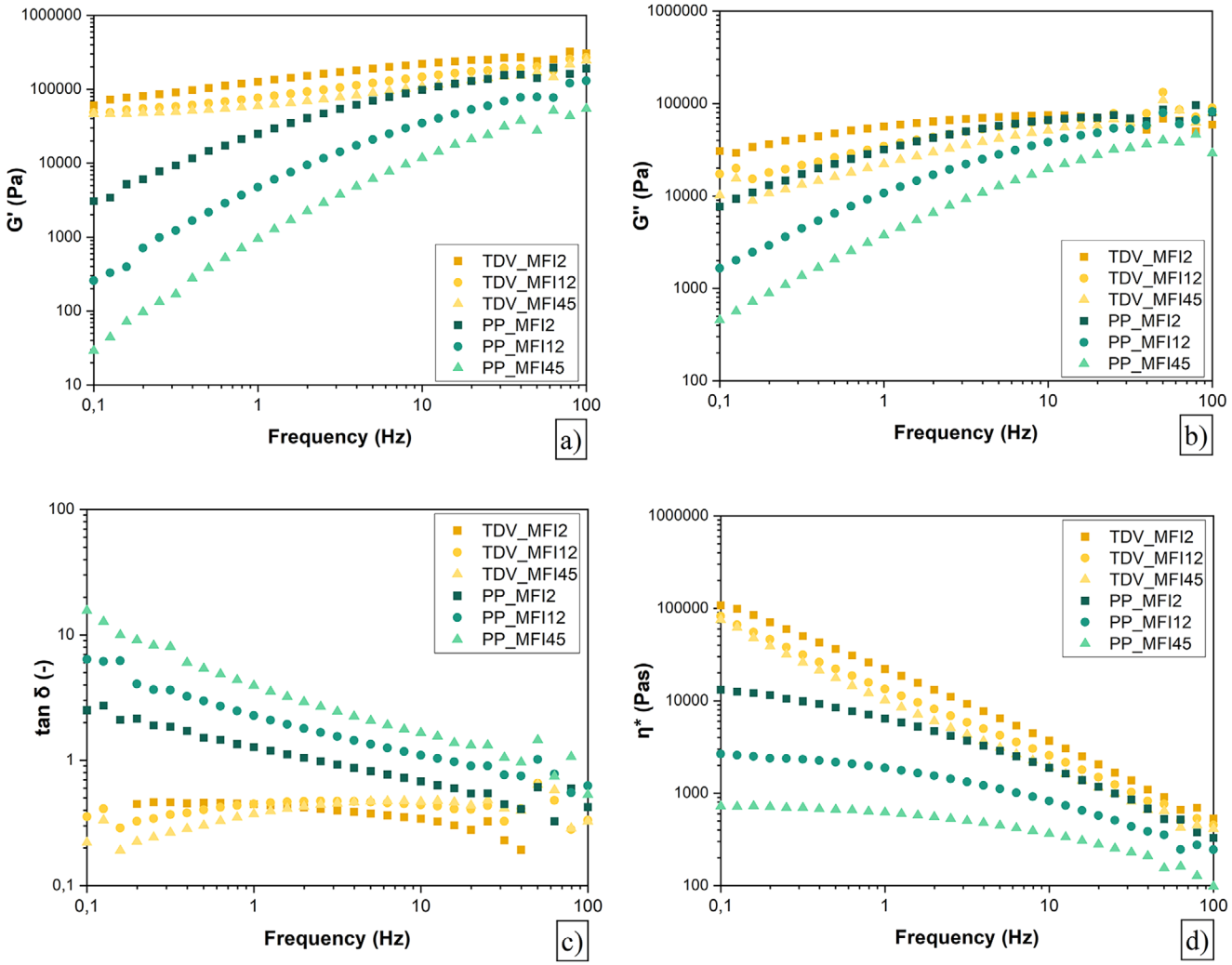

FIGURE 13 | Storage modulus (a), loss modulus (b), damping (c), and complex viscosity (d) curves of the PPs and TDVs.

to the better quality of rubber distribution. In addition, it is also observed that the linear viscoelastic section of TDV_MFI2 is wider than others. This indicates a better dispersion of the rubber phase and a better stability of the structure.

Figure 13 shows the storage and loss moduli of the samples along with their viscosity curves. In G' curves (Figure 13/a), the storage modulus of the TDVs does not change as much as that of the PPs with increasing frequency. This may indicate that the dispersed rubber particles dominate the viscoelastic behavior. The behavior of the cross-linked filler does not depend on the frequency, so this implies an established network that can be formed by particle-particle interactions. On the other hand, G'' of the TDVs (Figure 13/b shows similarities to the PPs; it increases with increasing frequency. However, for the TDVs, G'' increases less sharply with frequency, indicating better damping resulting from energy dissipation of the rubber phase. The effect of matrix viscosity is also evident in this respect: increasing viscosity leads to higher G'' and thus to higher energy dissipation. This effect is also visible on the damping curves (Figure 13/c: the TDVs have consistently lower values compared to PP samples, suggesting more elastic behavior in the melt state. The damping of TDVs is relatively flat across the frequency range, implying that the material's elastic-viscous balance does not change significantly with frequency due to a network of rubber particles. On the other hand, the damping of PP samples increases with frequency due to the transition from a more viscous to an elastic-dominated response as frequency increases, which is typical of thermoplastics.

The complex viscosity (Figure 13/d) of all TDVs decreases with increasing frequency. This indicates shear-thinning behavior and good processability, as these curves resemble the curves of polypropylenes. At low frequencies, TDVs exhibit larger viscosity and storage modulus compared to neat PPs; this indicates that TDVs are closer to ideal elastic networks in this region. This behavior is consistent with previous studies on traditional TDVs, where authors described that rubber particles tend to undergo physical clustering at low shear rates [50].

The Cole-Cole plot is a tool to assess multiphase blends and the relaxation spectrum of the phases. The diagrams for PPs (Figure 14/a) are characterized by the semi-circularity typical of thermoplastic polymers. As the MFI increases, the semicircular curve moves closer to the origin of the diagram. This suggests that PP_MFI2 may have the highest molecular weight, thereby the

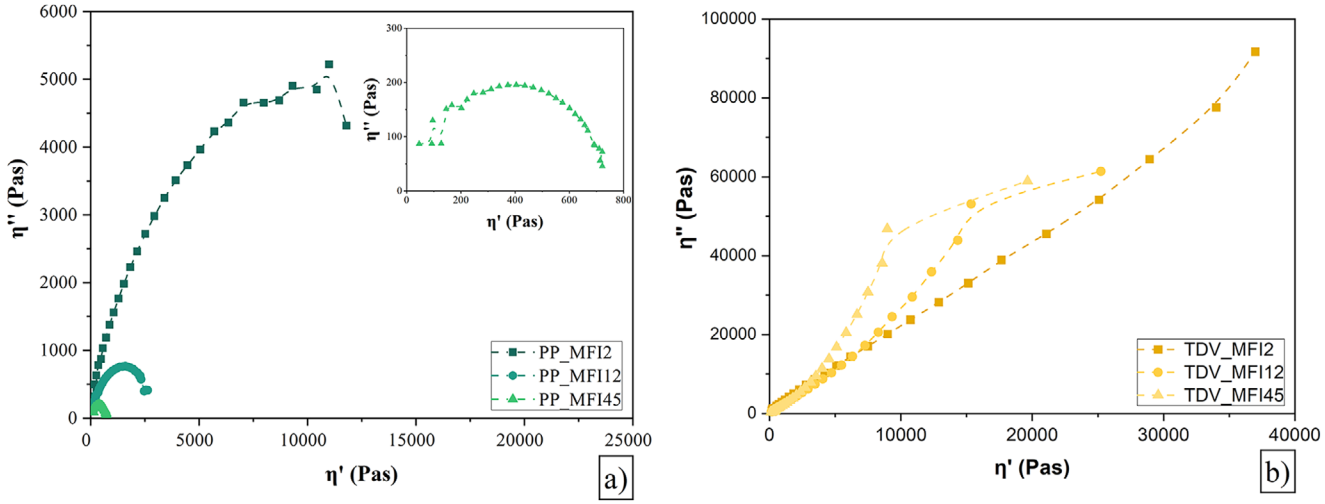

FIGURE 14 | Cole–Cole plots of the neat PPs (a) and the TDVs (b).

longest relaxation time. The Cole-Cole plots of TDVs (Figure 14/b) do not follow those of neat PPs as TDVs are characterized by linearity instead of semi-circularity. This confirms the previously seen tendency that the materials do not exhibit traditional viscoelastic behavior due to the different relaxation times of the rubber particles dispersed in large volumes. In addition, this behavior may also suggest that the material is characterized by particles and aggregates of different size ranges (with different relaxation times), as can be seen in the morphological analysis (Figure 4 and Figure 5). Comparing the Cole–Cole plots of the three TDVs also reveals the effect of matrix viscosity in this aspect. The slope increases with decreasing matrix viscosity, thus showing that loss viscosity dominates over elasticity. This can be attributed to the more favorable grain structure due to the increase in viscosity. In addition, the shape of the plots changes: TDV_MFI12 and TDV_MFI45 exhibit an arc at high viscosities. This may suggest that the relaxation characteristic of the rubber phase in these materials is different from that of the matrix (along with their viscosity), resulting in poorer cooperation between phases.

4 | Conclusions

We investigated the effect of matrix viscosity on thermoplastic dynamic vulcanizates made from devulcanized ground tire rubber and polypropylene. We have found that the increase in viscosity resulted in better dispersion of the rubber phase through increased shear generated by the melt, leading to an improvement in the main mechanical properties of TDVs.

The change in viscosity of the phases as a function of temperature was studied, as the two components behave in opposite ways in this respect. Based on these investigations, we have defined a temperature-dependent viscosity ratio that can be used to more accurately describe the viscosity ratio of the two phases and can be used to quantify the process window for dynamic vulcanization. On this basis, we have shown how increasing the scorch viscosity ratio improves strain at break, tensile strength, and perforation energy. We have also studied the failure behavior of the TDVs with acoustic emission, showing that decreasing the size of the rubber domains results in improved toughness, indicated by the change in signal properties.

The rheological properties of the materials were also investigated. We have shown that higher matrix viscosity provides an increasing linear viscoelastic range through a network of better-distributed rubber particles. The effect of matrix viscosity was also observed on the frequency dependence: the use of PP with the highest viscosity was shown to increase the stability and elasticity of the TDV structure. We also used Cole-Cole plots to understand the melt rheology better and found that increasing matrix viscosity results in a dominantly elastic behavior and closer relaxation characteristics to the rubber phase.

Acknowledgements

Project no. KDP-IKT-2023-900-I1-00000957/0000003 has been implemented with the support provided by the Ministry of Culture and Innovation of Hungary from the National Research, Development and Innovation Fund, financed under the KDP-2023 funding scheme. This research was funded by the National Research, Development and Innovation Office, Hungary (2021-1.1.4-GYORSÍTÓSÁV-2022-00030). Project no. TKP-6-6/PALY-2021 has been implemented with the support provided by the Ministry of Culture and Innovation of Hungary from the National Research, Development and Innovation Fund, financed under the TKP2021-NVA funding scheme.

Conflicts of Interest

The authors declare no conflicts of interest.

Data Availability Statement

The data that support the findings of this study are available from the corresponding author upon reasonable request.

References

1. D. Gere and T. Czigany, "Future Trends of Plastic Bottle Recycling: Compatibilization of PET and PLA," *Polymer Testing* 81 (2020): 106160.

2. F. Ronkay, B. Molnar, D. Gere, and T. Czigany, "Plastic Waste from Marine Environment: Demonstration of Possible Routes for Recycling by

Different Manufacturing Technologies," *Waste Management* 119 (2021): 101.

3. M. S. Abbas-Abadi, M. Kusenberg, H. M. Shirazi, B. Goshayeshi, and K. M. Van Geem, "Towards Full Recyclability of End-of-Life Tires: Challenges and Opportunities," *Journal of Cleaner Production* 374 (2022): 134036.

4. K. Formela, "Sustainable Development of Waste Tires Recycling Technologies–Recent Advances, Challenges and Future Trends," *Advanced Industrial and Engineering Polymer Research* 14 (2021): 209–222.

5. H. Chittella, L. W. Yoon, S. Ramarad, and Z.-W. Lai, "Rubber Waste Management: A Review on Methods, Mechanism, and Prospects," *Polymer Degradation and Stability* 194 (2021): 109761.

6. A. Fazli and D. Rodrigue, "Recycling Waste Tires Into Ground Tire Rubber (GTR)/Rubber Compounds: A Review," *Journal of Composites Science* 4 (2020): 103.

7. N. Candau, R. Leblanc, and M. L. Maspoch, "A Comparison of the Mechanical Behaviour of Natural Rubber-Based Blends Using Waste Rubber Particles Obtained by Cryogrinding and High-Shear Mixing," *Express Polymer Letters* 17 (2023): 1135.

8. X. Colom, M. R. Saeb, and J. Cañavate, "Microstructural Phenomena in Ground Tire Rubber (GTR) Devulcanized via Combined Thermochemomechanical and Microwave processes Monitored by FTIR and DTGA Assisted by Other Techniques," *Express Polymer Letters* 18 (2024): 950–961.

9. J. Karger-Kocsis, L. Mészáros, and T. Bárány, "Ground Tyre Rubber (GTR) in Thermoplastics, Thermosets, and Rubbers," *Journal of Materials Science* 48 (2013): 1.

10. K. Formela, J. Korol, and M. R. Saeb, "Interfacially Modified LDPE/GTR Composites with Non-Polar Elastomers: From Microstructure to Macro-Behavior," *Polymer Testing* 42 (2015): 89.

11. A. Fazli and D. Rodrigue, "Effect of Ground Tire Rubber (GTR) Particle Size and Content on the Morphological and Mechanical Properties of Recycled High-Density Polyethylene (rHDPE)/GTR Blends," *Recycling* 6 (2021): 44.

12. A. Kohári and T. Bárány "Sustainable Thermoplastic Elastomers Based on Thermoplastic Polyurethane and Ground Tire Rubber," *Journal of Applied Polymer Science* 141 (2024): 56157.

13. M. Burelo, I. Gaytán, S. Gutiérrez, et al., "Recent Advances in Sustainable Degradation Processes of Elastomers: A Comprehensive Review," *Reviews in Environmental Science and Bio/Technology* (2025): 1–37.

14. A. Fazli and D. Rodrigue, "Waste Rubber Recycling: A Review on the Evolution and Properties of Thermoplastic Elastomers," *Materials* 13 (2020): 782.

15. A. Belhaoues, S. Benmesli, and F. Riahi, "Compatibilization of Natural Rubber–Polypropylene Thermoplastic Elastomer Blend," *Journal of Elastomers & Plastics* 52 (2020): 728–746.

16. A. J. Andrade and C. Saron, "Mechanical Recycling of Expanded Polystyrene and Tire Rubber Waste as Compatibilized and Toughened Blends," *Journal of Applied Polymer Science* 140 (2023): 54267.

17. S. Liu, Z. Peng, Y. Zhang, D. Rodrigue, and S. Wang, "Compatibilized Thermoplastic Elastomers Based on Highly Filled Polyethylene with Ground Tire Rubber," *Journal of Applied Polymer Science* 139 (2022): 52999.

18. D. Á. Simon and T. Barany, "Effective Thermomechanical Devulcanization of Ground Tire Rubber with a Co-Rotating Twin-Screw Extruder," *Polymer Degradation and Stability* 190 (2021): 109626.

19. S. Seghar, L. Asaro, M. Rolland-Monnet, and N. A. Hocine, "Thermo-Mechanical Devulcanization and Recycling of Rubber Industry Waste," *Resources, Conservation and Recycling* 144 (2019): 180.

20. H. Yazdani, M. Karrabi, I. Ghasmi, H. Azizi, and G. R. Bakhshandeh, "Devulcanization of Waste Tires Using a Twin-Screw Extruder: The Effects of Processing Conditions," *Journal of Vinyl and Additive Technology* 17 (2011): 64.

21. A. Rodak, J. Haponiuk, S. Wang, and K. Formela, "Investigating the Combined Effects of Devulcanization Level and Carbon Black Grade on the SBR/GTR Composites," *Express Polymer Letters* 18 (2024): 1191.

22. J. I. Gumede, B. G. Hlangothi, C. D. Woolard, and S. P. Hlangothi, "Organic Chemical Devulcanization of Rubber Vulcanizates in Supercritical Carbon Dioxide and Associated Less Eco-Unfriendly Approaches: A Review," *Waste Management & Research* 40 (2022): 490.

23. D. Á. Simon and T. Bárány, "Microwave Devulcanization of Ground Tire Rubber and Its Improved Utilization in Natural Rubber Compounds," *ACS Sustainable Chemistry & Engineering* 11 (2023): 1797–1808.

24. O. Buitrago-Suescún, R. Britto, "Devulcanization of Ground Tire Rubber: Thermo-Oxidation Followed by Microwave Exposure in the Presence of Devulcanizing Agent," *Iranian Polymer Journal* 29 (2020): 553.

25. A. S. Mohite, Y. D. Rajpurkar, and A. P. More, "Bridging the Gap Between Rubbers and Plastics: A Review on Thermoplastic Polyolefin Elastomers," *Polymer Bulletin* 79 (2021): 1309.

26. J. G. Drobny, *Handbook of Thermoplastic Elastomers*, 2nd Ed. (Elsevier Inc, Oxford, 2014).

27. N. Ning, S. Li, and H. Wu, "Preparation, Microstructure, and Microstructure-Properties Relationship of Thermoplastic Vulcanizates (TPVs): A Review," *Progress in Polymer Science* 79 (2018): 61.

28. N. Ghahramani, K. A. Iyer, A. K. Doufas, and S. G. Hatzikiriakos, "Rheology of Thermoplastic Vulcanizates (TPVs)," *Journal of Rheology* 64 (2020): 1325.

29. C. Nakason, C. Manleh, N. Lopattananon, and A. Kaesaman, "The influence of Crosslink Characteristics on Key Properties of Dynamically Cured NR/PP Blends," *Express Polymer Letters* 18 (2024): 487.

30. A. Kohári, I. Z. Halász, and T. Bárány, "Thermoplastic Dynamic Vulcanizates with In Situ Synthesized Segmented Polyurethane Matrix," *Polymers* 11 (2019): 1663.

31. T. Bárány, A. Kohári, D. Á. Simon, D. Kocsis, and I. Z. Halász *Periodica Polytechnica Chemical Engineering* 64 (2019): 248.

32. N. Candau, N. L. Albiter, H. Jeannot, and M. L. M. Ruldua, "Dynamically Vulcanized Polylactic Acid/Natural Rubber/Waste Rubber Blends: Effect of the Rubber Content," *Journal of Materials Science* 57 (2022): 17902.

33. P. S. Garcia, J. A. d. Lima, C. H. Scuracchio, and S. A. Cruz, "The Effect of Adding Devulcanized Rubber on the Thermomechanical Properties of Recycled Polypropylene," *Journal of Applied Polymer Science* 138 (2021): 50703.

34. Á. Görbe, P. Széplaki, and T. Bárány, "Ultrasonic Welding of Ground Tire Rubber-Filled Polypropylene Blends," *Results in Engineering* 25 (2025): 104588.

35. R. Babu, N. K. Singha, and K. Naskar, "Interrelationships of Morphology, Thermal and Mechanical Properties in Uncrosslinked and Dynamically Crosslinked PP/EOC and PP/EPDM Blends," *Express Polymer Letters* 4 (2010): 197.

36. C. Nakason, M. Jarnthong, A. Kaesaman, S. Kiatkamjornwong, "Influences of Blend Proportions and Curing Systems on Dynamic, Mechanical, and Morphological Properties of Dynamically Cured Epoxidized Natural Rubber/High-Density Polyethylene Blends," *Polymer Engineering & Science* 49 (2009): 281.

37. C. Antunes, A. Machado, and M. Van Duin, "Morphology Development and Phase Inversion During Dynamic Vulcanisation of EPDM/PP Blends," *European Polymer Journal* 47 (2011): 1447.

38. X. Zhang, H. Huang, and Y. Zhang, "Dynamically Vulcanized Nitrile Rubber/Polypropylene Thermoplastic Elastomers," *Journal of Applied Polymer Science* 85 (2002): 2862.

39. G. Z. Marton and G. Szebényi, "Influencing the Damage Process and Failure Behaviour of Polymer Composites—A Short Review," *Express Polymer Letters* 19 (2025): 140.

40. G. Z. Marton, F. Balogh, and G. Szebényi, "Acoustic Emission Analysis and Signal Classification for Damage Modes in UD Carbon/Epoxy Composites," *Express Polymer Letters* 19 (2025): 809.

41. J. Bohse, "Acoustic Emission Characteristics of Micro-Failure Processes in Polymer Blends and Composites," *Composites Science and Technology* 60 (2000): 1213.

42. Á. Görbe, G. Z. Marton, and T. Bárány, "Acoustic Emission Analysis of Failure Processes in Polyethylene and Recycled Tire Rubber Blends," *Polymer Testing* 147 (2025): 108813.

43. T. Bremner, A. Rudin, and D. G. Cook, "Melt Flow Index Values and Molecular Weight Distributions of Commercial Thermoplastics," *Journal of Applied Polymer Science* 41 (1990): 1617.

44. T. Bremner, D. Cook, and A. Rudin, "Further Comments on the Relations Between Melt Flow Index Values and Molecular Weight Distributions of Commercial Plastics," *Journal of Applied Polymer Science* 43 (1991): 1773.

45. E. E. Ferg and L. L. Bolo, "A Correlation Between the Variable Melt Flow Index and the Molecular Mass Distribution of Virgin and Recycled Polypropylene Used in the Manufacturing of Battery Cases," *Polymer Testing* 32 (2013): 1452.

46. N. Ning, L. Hu, P. Yao, et al. *Journal of Applied Polymer Science* (2015): 133.

47. H. Wu, M. Tian, and L. Zhang, et al., "Effect of Rubber Nanoparticle Agglomeration on Properties of Thermoplastic Vulcanizates During Dynamic Vulcanization," *Polymers* 8 (2016): 127.

48. S. S. Banerjee and A. K. Bhowmick, "Dynamic Vulcanization of Novel Nanostructured Polyamide 6/ Fluoroelastomer Thermoplastic Elastomeric Blends with Special Reference to Morphology, Physical Properties and Degree of Vulcanization," *Polymer* 57 (2015): 105.

49. J. Karger-Kocsis, "Thermoplastic Rubbers via Dynamic vulcanization," *Polymer Blends and Alloys* (Routledge, 2019): 125.

50. R. M. A. L'Abee, "Thermoplastic Vulcanizates: The Rubber Particle Size to Control the Properties-Processing Balance. *PhD thesis*, Technische Universiteit Eindhoven (2009)".